8-17-2020

Underground Phased Arrays and Beamforming Applications

Abdul Salam
Purdue University, salama@purdue.edu

Usman Raza
Purdue University

Chapter 7
Underground Phased Arrays and Beamforming Applications

Abstract This chapter presents a framework for adaptive Beamforming in underground communication. The wireless propagation is thoroughly analyzed to develop a model using the soil moisture as a input parameter to provide feedback mechanism while enhancing the system performance. Working of array element in the soil is analyzed. Moreover, e ect of soil texture and soil moisture on the resonant frequency and return loss is studied in detail. The wave refraction from the soil-air interface highly degrades the performance of the system. Furthermore, to beam steering is done to achieve high gain for lateral component improving the UG communication. The angle enhancing the lateral wave depends upon dielectric properties and usually range from $0°$ to $16°$. These dielectric properties changes with the change in soil moisture and and soil texture. It is shown from the experiments that optimal UG lateral angle is high at lower soil moisture readings and decreases with decrease in soil moisture. A planar structure of antenna array and di erent techniques for optimization are proposed fro enhanced soil moisture adaptive beamforming. UG channel impulse response is studied from the beamforming aspect to identify the components of EM waves propagating through the soil. An optimum steering method for beamforming is presented which adapts to the changing values of soil moisture. Finally, limitations of UG beamforming is presented along-with the motivation to use it.

7.1 Introduction

Underground (UG)communication is highly e ected by the soil properties [59]. Limited communication range (($8\,\mathrm{m}$ to $12\,\mathrm{m}$)) due to high soil attenuation still remains the biggest challenge even after the developments in wireless communication[52], [56], [139], [62], [59], [50], [58], [72]. Therefore, an adaptive UG communication system, with integrated sensing and communication system, is needed which dynamically changes the communication parameters with change in environment. It is required to change the antenna parameters (operation frequency and bandwidth) for changing

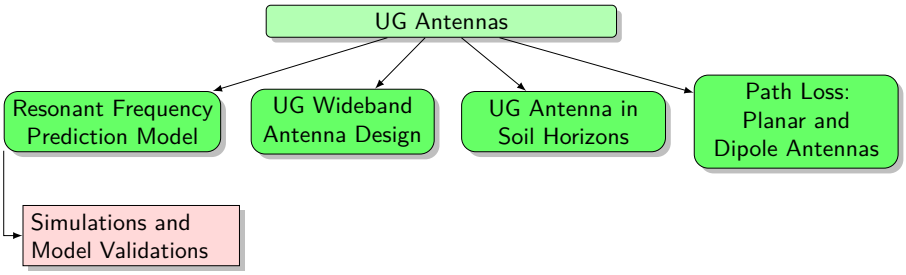

Fig. 7.1: Organization of the Chapter

soil moisture[62]. The contribution of lateral waves is enhanced by directing the energy at a particular angle. The angel is determined by the nearby environment in which the UG antenna is buried[59]. Therefore, using the antenna without an ability to direct its beam direction causes the system performance to degrade, hence, a soil moisture adaptive beamforming technique is required for high throughput and gain.

It is shown in [59] that lateral waves Lateral waves are the dominant component of the signal in UG communication [52], [54], [69]. The lateral waves has the ability to carry the most energy and achieve high communication range, if antennas are aligned at particular angle. The angel varies the variation in soil moisture, soil texture and bulk density. On the other hand, antenna also needs to be vertically aligned to prevent the refraction at the soil-air interface.

There are many factors which can e ect the beamforming of antenna arrays. Some of the factor includes: distance of antenna elements from soil-air interface, delay in speed beams causes refractive indices to change, soil moisture causing resonant frequency to change which in-turn changes the bandwidth return loss and reflection coefficient. The beamforming un UG2UG and UG2AG di ers such that former requires lateral waves to travel along soil-air interface and later is focused on broadside. Due to di erent nature of propagation in both links, di erent angels are used for the links. Therefore, phase is adjusted at UG antenna elements for coherent addition to avoid errors in beam pointing direction. SMABF achieves high performance by aligning the signal envelops. It is important to understand the propagation in wireless UG communication to develop a reliable beamforming architecture and advanced mechanism are needed extend the communication range. Therefore, optimum beamforming technique requires to determine the accurate physical characteristics of wireless UG channel propagation . Soil moisture adaptive beamforming (SMABF) uses an underground antenna array for communication through the soil. As per receiver position, the EM waves either goes completely or partially through the soil. In partial case, come of it propagates through air. A beamformingBeamforming method is developed using the optimal angle. An optimization algorithm is proposed which works on the feedback given by the soil moisture sensors Soil moisture sensors.

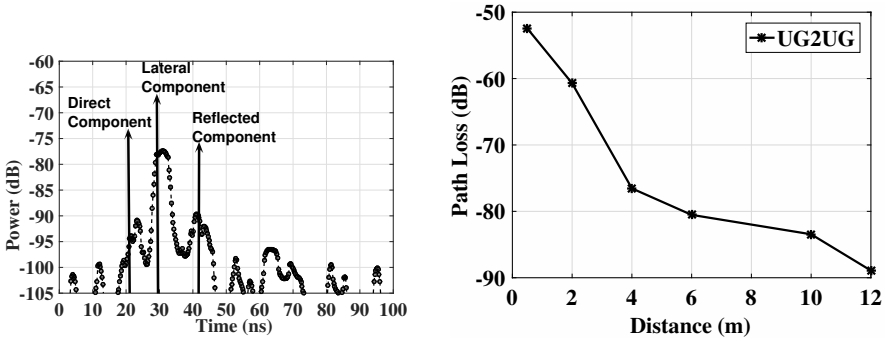

(a) (b)

Fig. 7.2: (a) Power delay profile (PDP) [50], (b) Pathloss in UG2UG channel [50]

SAMBF is applied in various applications such as: ground penetrating radars (GPR) Ground penetrating radars (GPR), locating IEDs, aircraft communication from the runway, precision agriculturePrecision agriculture, hazardous object search, geology, and wireless underground sensor networks (WUSNs) Wireless Underground Sensor Networks (WUSNs). Specifically, WUSNs uses both electromagnetic (EM) [177] and Magnetic Induction-based propagation [170] and are being applied in land slide monitoring, and Pipeline monitoring [70], precision agriculture [9, 52, 58, 74, 75, 100, 164], border monitoring [54, 71, 75, 164].

A special beamforming antenna have been introduce and being used in wireless to achieve reduced interference and increased capacity. There has been e ort in the literature for exploring OTA channel beamforming techniques [3, 4, 5, 11, 23, 24, 27, 28, 79], and MI-power transfer [21]. However, there has been no e orts made to realize the beamforming in UG communications. Lateral component [19] in UG communication can be improved further, via beamforming, to achieve long range communication.

7.2 Channel Model for SMABF

It is important to completely understand the wave behavior in soil while designing the UG communication system. A UG channel model is give in [59] which identify three major components namely: Direct Direct Waves, lateralLateral Waves and reflected components Reflected Waves at the receiver. It can be seen in the Direct Wavespower delay profile (Fig. 7.2(a)) that lateral wave is the strongest component as it travels most of the time through soil interface.

These factors contribute to the failure of using impedance matched antennaImpedance matched antenna used for OTA to be used in soil motivating for developing new designs. Moreover, isotropic signal radiation will result in resource wastage because of buried deployment. Therefore, SMABF forms a focused narrow

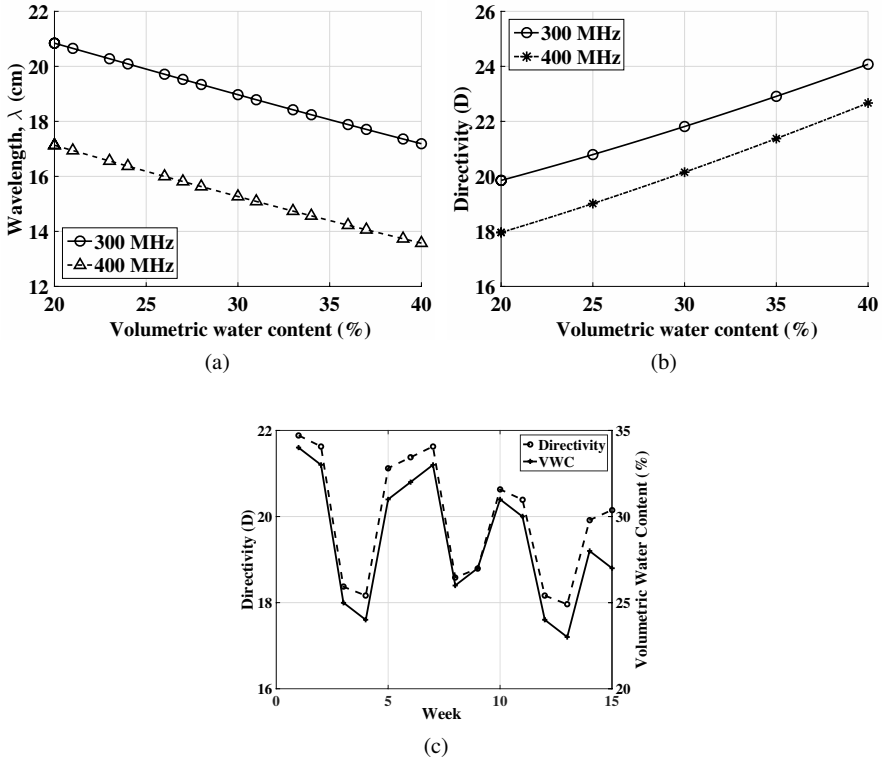

Fig. 7.3: (a) Wavelength as a function of soil moisture [50] (b) Array directivity as a function of soil moisture [50], (c) Antenna directivity for soybean field during growing season

beam for communication between UG and AG devices to extend the communication range.

As given in [59], a UG channel can be given as sum of all wave components as follow:

$$h_{ug}(t) = \sum_{l=0}^{L-1} \alpha_l \delta(t-\tau_l) + \sum_{d=0}^{D-1} \alpha_d \delta(t-\tau_d) + \sum_{r=0}^{R-1} \alpha_r \delta(t-\tau_r)\,, \tag{7.1}$$

where subscripts L, D, and R refers to lateral, direct and reflected components, α is the complex gain and τ is the delays of each corresponding component.

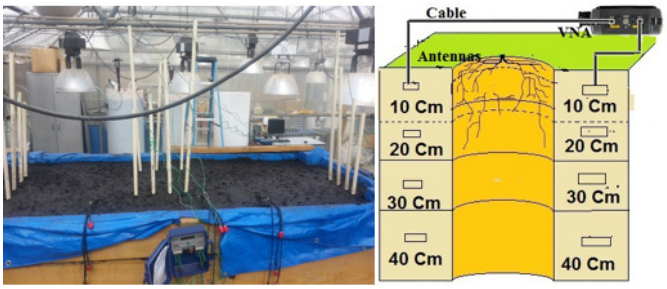

Fig. 7.4: Layout of the indoor Testbed [51]

7.2.1 Unique Features of UG Channel

Underground medium is considered unique and di erent form other medium because of combined interaction between soil Soil, antennas and channel. In soil wavelengthWavelength of a signal is relatively lower than air because of relatively higher permittivityPermittivity than air. Hence, for less attenuation, lower frequencies are used with small antenna in UG communication. This is beneficial because it permits the use of reasonably sized underground antenna array. Furthermore, in Fig. 7.2(a), decreasing the delay spread can result in long-range communication with high data rates.

UG communicationsu ers from (1) short-range of communication and (2) low data rate. Short range is due to the signal su ering from high attenuation in the soil as shown in Fig. 7.2(b). In Fig. 7.2(b), it is shown that path loss increases (30 dB increase) with increase in distance from 2m to 12m. Moreover, in [62], a low data rate is observed in UG communication with commodity motes. These limitations are dealt by using SMABF.

7.2.2 Underground Beamforming - Research Challenges

This section lists the challenges observed in underground beamforming.

Analyzing effect of soil moisture on signal wavelength:

Wavelength of a signal propagating in the soil is given as:

$$\lambda_s = \frac{2\pi}{k_s} \tag{7.2}$$

where k_s gives the wave number in soil.

Fig. 7.3(a) plots wavelength with soil moisture. It can be seen that, at 300 MHz, wavelength decreases from 21cm to 17cm for a soil moisture decrease of 20 to 40%. Similarly, at 400 MHz, it decreases from 17cm to 14cm. Therefore, it is important to maintain the inter-element distance in such a way that wavelength change can be accommodated for sudden changes of soil moisture without e ecting the beam pattern.

Analyzing effect of soil moisture on directivity:

Directivity is calculated by using the equation in [17]:

$$D \approx 2\frac{Nd}{\lambda_s} \tag{7.3}$$

where N denotes the number of elements, d inter-element distance, and λ_s gives the wavelength in soil.

Fig. 7.3(b) plots directivity with soil moisture. This graph is for the inter-element distance of half wavelength $\lambda_0/2$. antenna element. Similarly, Fig. 7.3(c) shows the measurement of directivity using 4-antenna element for 15 weeks of soil moisture data. The data was collected in 2015 from soy bean field during summer. The figures shows that directivity changes dynamically with the change in soil moisture. This e ects requires mitigation through SMABF.

The antenna beam can be steered using the phased arrays that too without having any physical movement [13, 15, 18]. In UG communication, wavelength is continuously changing and needs an accurate phase control. Therefore, smart antenna with phase shifters suits the UG communication application. Wideband antenna arraysmay face the space and hardware issues while deployment in underground communication. Limited closed-form antenna models for UG environment makes it difficult to understand the UG beamforming. In coming sections, soil e ects on UG beamforming are studied to design an efficient SMABF technique with an aim to maximize the communication range and data rate.

7.2.3 Analysis of Single Array Element in Soil

Firstly, an empirical comparative analysis of a single soil antenna element with that of OTA antenna element is done in testbed shown in Fig. 7.4. This testbed deploy antenna using di erent depth and distance values and analyzes the e ect of soil-air interface and impedance of antenna element.

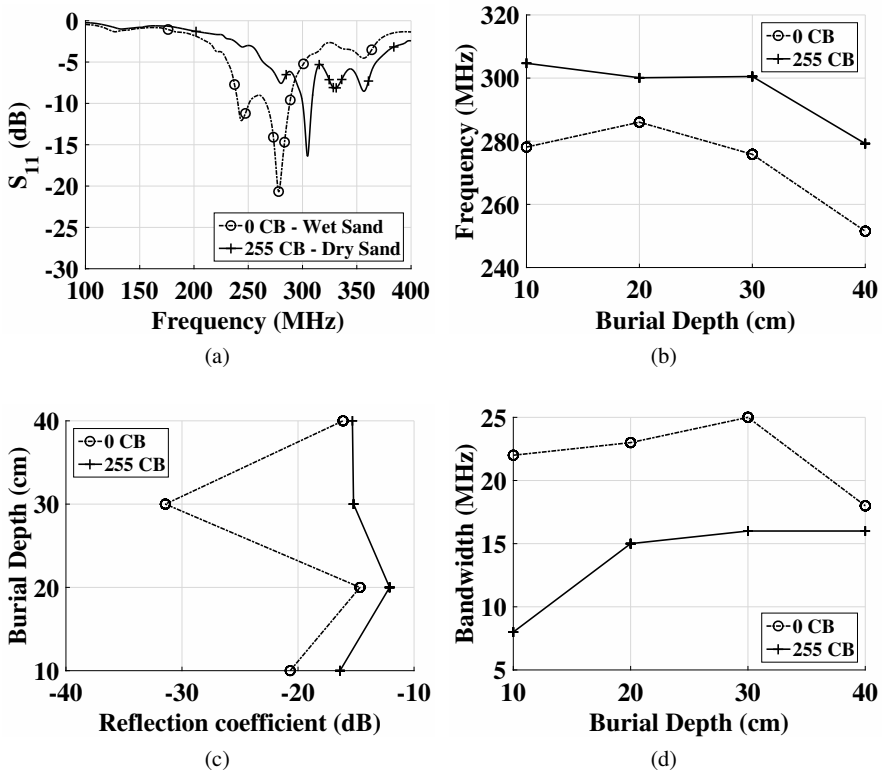

Fig. 7.5: (a) E ect of frequencies on return loss [50], (b) E ect of depth on resonant frequencies with varying soil moisture [50], (c) E ect of depth on Reflection Coefficient (dB) at di erent burial depths, (d) E ect of depth on bandwidth [50]

Table 7.1: Performance of 433 MHz OTA dipole antenna in soil

Property	**Soil**
Resonant Frequency	Increases with the increase in soil moisture Increases with the increase in burial depth
Wavelength	Decreases with the increase in soil moisture
Return Loss	Decreases with the increase in soil moisture

In-Soil v/s OTA Array Element

This section presents the comparison of UG dipole antenna element with antenna element in free space. The frequency is varied from 100 to 500 MHz. It can be seen

that resonant frequency decreases because of shorter wavelength in the soil. Thee resonant frequency is 202 MHz, 209 MHz, and 278 MHz in silt loam soil, silty clay loam and in sandy soil, respectively. It is interesting to note that resonant frequency of sandy soil is higher than that of silt loam soil due to lower water holding capacity [7].

Effect of Soil Moisture on individual antenna element return loss S_{11}

Fig. 7.5(a) plots the return loss Return Loss with frequency for varying soil moisture value from 0 to 255 CB. The experiment is performed using depth of 10 cm in silt loam soil. It can be seen that decrease in soil moisture causes the resonant frequency to increase from 278 t 305 MHz.

Fig. 7.5(b) plots the resonant frequency Resonant Frequency with burial depth for varying soil moisture values from 0 to 255 CB. For a given depth value, the resonant frequency increases with change in soil moisture. For example, at the depths of 20 cm resonant frequency increases from what it is at 10 cm to 276 MHz when soil moisture changes from 0 to 255 CB. Similar trend is observed for all other depths where resonant frequency increases from the previous depth when soil moisture is varied from 0 to 255 CB.

Fig. 7.5(a) to 7.5(d)) analyses the return loss of an antenna for di erent depths and soil moisture values. It is observed that return loss and resonant frequency are a ected by the change in soil moisture values. Furthermore, in contrast to OTA communication, optimal frequency is also di erent from the antenna resonant frequency [62].

Antenna Element Impedance in Soil

Input impedance Z_a of antenna element should be matched with output impedance of radio transceiver Z_s to achieve robust and efficient wireless communication. the matching is performed in such a way that maximum power is radiate and minimum power is transmitted back at the transmitter. In contrast to OTA medium, soil is not an infinite medium because of soil-air interface e ect. Accordingly, return loss of an antenna RL is not just a spectrum shift but RL curve shape is also di erent.

Soil-Air Interface Impacts

On exciting the antenna, the current distribution of $I_0(\zeta)$ is generated from the antenna and travel towards soil-air interface where it is reflected and refracted. The reflected electric field E_r travel back to antenna where it induces and additional current I_r and e ect the impedance of antenna [71]. I_r causes higher order of reflection e ect, however, it can be ignored because of high attenuation in the soil,

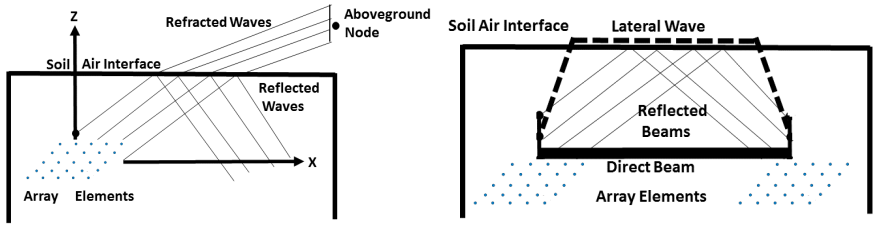

(a) (b)

Fig. 7.6: Communications schematic for [50]: (a) UG2AG communications (b) UG2UG communications

hence, only first-order e ect is considered. Induced current I_r and impedance due to this induced current Z_r can be modeled considering an imaginary dipole placed in the soil environment. Similarly, Z_r is modeled as the mutual impedance from two dipole antennas [25] and reflection coefficient of soil-air interface. the mutual impedance Z_r along with self impedance Z_a gives the total impedance of buried antenna in half space [71].

Using the results from the analysis of individual antenna element, design of multi-element SMABF array is presented in coming sections.

7.3 Design of SMABF Array

The section will discuss the beamforming technique in context of UG2UG and UG2AG communication. Basic concepts of beamforming are not discussed here and readers are encouraged to refer [14] for details on Beamforming basic tutorial.

7.3.1 Array Layout and Element Positioning

SMABF antenna array is expected to have following characteristics:

1. Spacing between the antennas should consider the soil e ect on wavelength of the soil. It should be done in such a way that desired beam shape and directivity should not be lost because of soil e ects.
2. It should be able to work with wide range of frequencies.
3. Elements should be half-wavelength and support multiple inter-element spacing.
4. High number of elements provide high directivity. However, to determine number of array elements, one should also consider the UG deployment conditions. Therefore, total number must be easy to deploy and maintains high directivity.
5. Array patterns should support the steering angle. This applies to both UG2UG and UG2AG antenna arrays.

Table 7.2: Steering Angles

Communication Link	θ	ϕ
UG2AG - No Steering	$0°$	$0°$
UG2AG - Beam Steering	$0° - 60°$	$0°$
UG2UG - Lateral Wave	VWC Dependant See Section 7.3.3	$0°$
UG2UG - Direct Wave - X Orientation	$90°$	$0°$
UG2UG - Direct Wave - Y Orientation	$90°$	$90°$

6. It should be adaptive to changes in soil moisture.

Multi-dimensional arrays structure, e.g., rectangular, planar, and circular has an advantage of providing simultaneous beams in more than one planes [13]. To fulfill the requirement of di erent array patterns, SMABF uses the planar array structure. The array lie on $x - y$ plane and its $z-$ plane points toward the soil-air interface. Elevation angle θ is measure for AG node and azimuthal angle ϕ is measured for the UG node. θ is measured from normal to soil-air interface whereas ϕ measures steer beams to UG nodes. Table 7.2 lists the beam steering angles for UG2AG and UG2UG communication links. Planar antenna array is shown in Fig. 7.7(a).

Planar antenna array has an advantage of providing customized and desired radiation pattern. This customization is useful for communicating with AG nodes. Moreover, antenna elements are divided into multiple array groups on the basis of source strength. In this way source strength can be adjusted to make the lateral wave component stronger depending upon the depth and attenuation in vertical direction [20], [19].

Underground Communication Links

Fig. 7.6 shows the communication schematic where UG nodes communicate with UG and AG nodes via UG2UG and UG2AG links, respectively. AG nodes are can either be fixed or mobile. For AG communication, waves are reflected from soil-air interface and lateral waves are used in UG communication. The desired beam pattern is given in Fig.7.6. It is seen that for UG2AG communication, the EM waves reflected and refracted from soil-air interface which e ect the pattern towards AG node.

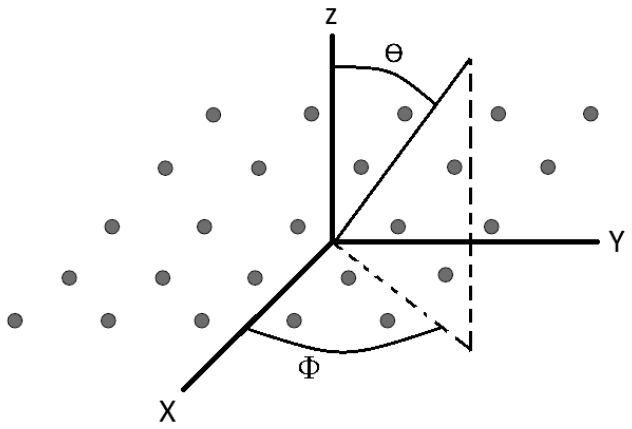

(a)

Fig. 7.7: Placements of antenna array elements in a 5×5 planar grid [50]

7.3.2 Beam Pattern for Underground to Aboveground (UG2AG) Communication

Di erence in UG2AG and AG2UG communication links requires to determine the energy from UG antenna at di erent receiver angels. To that end, experiments were conducted for varying angles to assess the UG to AG communication [59]. The burial depth of sender UG node is kept at 20cm and multiple distances of AG node, from the soil surface, were used. AG node is mounted at adjustable pole and distances were varied by changing the height. Following distances were used for the experiment: $2\,\mathrm{m}$, $4\,\mathrm{m}$, $5.5\,\mathrm{m}$, and $7\,\mathrm{m}$.

Following angles were used for the experiments are: $0°$, $30°$, $45°$, $60°$, and $90°$. Highest attenuation was observed at receiver angle $0°$ and lowest at $90°$. The reason for the lowest attenuation is because of no refraction from soil-air interface at $90°$. At $90°$, due to lowest wave refraction, the energy is directed towards soil-air interface, thus, gives high gains and throughput in UG communication. There can be three cases in UG communication which are discussed below:

1. *UG communication with No Steering* - For this case array factor for UG2AG pattern is given as follow [18]:

$$AF(\theta,\phi) = \sum_{i=1}^{N} w_i exp(-\big[jk_s r_i(x_i \sin\theta\cos\phi + y_i \sin\theta\sin\phi)\big]), \tag{7.4}$$

where w_i represents the weight of the antenna element, N denotes the total number of antenna elements, and x_i, y_i gives the location coordinate of $i-$th element in the array.

2. *UG communication with Beam Steering* - The no steering pattern can be used to create a broadside beam without considering the AG nodes location. However, with exact knowledge of AG node location, values for θ_{AG} and ϕ_{AG}, the beam can be steered by adding phase shifts δ_i at $i-th$ element. The element then can steer the beam to (θ_{AG},ϕ_{AG}) as follow:

$$AF(\theta,\phi) = \sum_{i=1}^{N} w_i exp(-\big[jk_s r_i(x_i \sin\theta\cos\phi + y_i \sin\theta\sin\phi)\big] + \delta_i),$$

where δ_i can be calculated as:

$$\delta_i = -k_s(x_i \sin\theta_{AG}\cos\phi_{AG} + y_i \sin\theta_{AG}\sin\phi_{AG})$$

3. *Refraction Adjustment* - When beam steering is performed at angles di erent from the normal ones, refraction becomes significant and cannot be ignored. It occurs because of wave coupling with soil-air interface. This interface separates soil from air and di erence in the properties of both medium causes refraction. Refraction not only deteriorate the UG beamforming performance but also causes the angle of arrival to change at AG nodes. Due to di erence in the medium properties, refraction causes delay due to di erent speed of the wave. This causes the spreading and decay of focused beam ultimately causing error in beam pointing direction and beam steering. This error due to refraction at soil-air interface is known as beam squint [18] resulting in signal dispersion.

SMABF deals with this issue by suing time-delay beam steering [18] which aligns the signal envelope. This reduces the e ects due to soil-air interface. Time delays and refraction angle are used for setting the beam direction. For an AG node location (θ_{AG},ϕ_{AG}), time delay is given as:

$$\emptyset_{\mathsf{mn}} = \begin{pmatrix} \tau_{11} & \tau_{12} & \dots & \tau_{1n} \\ \tau_{21} & \tau_{22} & \dots & \tau_{2n} \\ \vdots & \vdots & \ddots & \vdots \\ \tau_{m1} & \tau_{m2} & \dots & \tau_{mn} \end{pmatrix} \tag{7.5}$$

where τ_{ij} is given as:

$$\tau_{ij} = \sin\theta_r[i \times d_i \cos\phi_r + j \times d_j \sin\phi_r]/S, \tag{7.6}$$

where S denotes the speed of signal wave in soil, d_i is the element spacing in x direction and d_j in y direction. θ_r is estimated by Snell's law as follow:

$$\theta_r = \arcsin\left(\frac{\eta_s}{\eta_a}\sin\theta_{AG}\right), \tag{7.7}$$

where η_a and η_s are the refractive index of ar and soil, respectively.

τ_{ij}, in equation (7.6), depends upon the burial depth and soil moisture. Higher refraction index decreases the speed of the wave, hence, increasing the delay as well. After estimating τ_{ij} and δ_i, array factor is expressed as:

$$AF(\theta,\phi) = \sum_{i=1}^{N} w_i exp(-\big[jk_s r_i(x_i\sin\theta\cos\phi + y_i\sin\theta\sin\phi) + 2\pi f\sum_{j-1}^{M}\tau_{ij} + \delta_i\big], \tag{7.8}$$

7.3.3 UG2UG Communication Beam Pattern

There can be two scenarios for the communication between underground devices, i.e., UG2UG communication. Both scenarios are given below:

1. *Estimation of Soil Moisture-Based Optimum Steering Angle to Maximize Lateral Wave* - As discussed earlier, lateral waves travels along soil-air interface [61], [59]. These lateral waves can be maximized by adjusting the antenna radiation angle. The angle is based on the dielectric properties of soil and can be calculated as [67]:

$$\theta_{UG} = \frac{1}{2}\tan^{-1}\left(\frac{2Re(n^2-1)^{1/2}}{|n^2-1|-1}\right)rad, \tag{7.9}$$

where n is the soil refractive index and calculated as:

$$n = \sqrt{\frac{\sqrt{\epsilon\prime^2+\epsilon\prime\prime^2}+\epsilon\prime}{2}}, \tag{7.10}$$

In above equation, real and imaginary parts of soil permittivity Soil Permittivity are represented by $\epsilon\prime$ and $\epsilon\prime\prime$, respectively.

2. *Direct Wave* - Direct waves are the relatively prominent and dominant component in short-range UG communication. Therefore, short-range UG communication is improved through direct UG beam going towards the receiver.

The values for steering angle used in both cases are given in Table. 7.2 and equation (7.5) is for for direct and lateral case..

7.3.4 Directivity

Directivity of a SMABF array is calculate as:

$$D = \frac{4\pi |AF_{max}|^2}{\int_0^{2\pi} \int_0^{\pi} |AF|^2 \sin\theta d\theta d\phi}, \tag{7.11}$$

Algorithm 2 SMABF Beam Steering Algorithm

Initialization :

Let A be the set of AG nodes
Let U be the set of the UG nodes
Let R be the receiver node
Sense the soil moisture level and determine the appropriate wavelength in soil
Select the array layout based on wavelength
Activate desired elements based on soil moisture and desired beam patterns
Produce the initial weights to achieve the desired beam pattern
Calculate the excitation and current distribution (root matching, pole-residue)
BEGIN
if R $\in$ A then **then**
    if θ_R is known **then**
        $AF(\theta,\phi) = \sum_{i=1}^{N} w_i exp(-\left[jk_s r_i(x_i \sin\theta\cos\phi + y_i \sin\theta\sin\phi)\right] + \delta_i)$
    else if
      then
        Normal to the surface beam using
$AF(\theta,\phi) = \sum_{i=1}^{N} w_i exp(-\left[jk_s r_i(x_i \sin\theta\cos\phi + y_i \sin\theta\sin\phi)\right])$,
    end if
else if R $\in$ U **then**
    BEGIN
    Sense soil moisture
    Determine optimal angle using
$\theta_{UG} = \frac{1}{2}\tan^{-1}\left(\frac{2Re(n^2-1)^{1/2}}{|n^2-1|-1}\right)$
    Output UG2UG Beam
    END
end if
Optimize to get low side lobe levels when wavelength changes
Optimize element positions
Activate virtual arrays
Adjust weights and excitation
Repeat this process to adjust these parameters when soil moisture changes
END

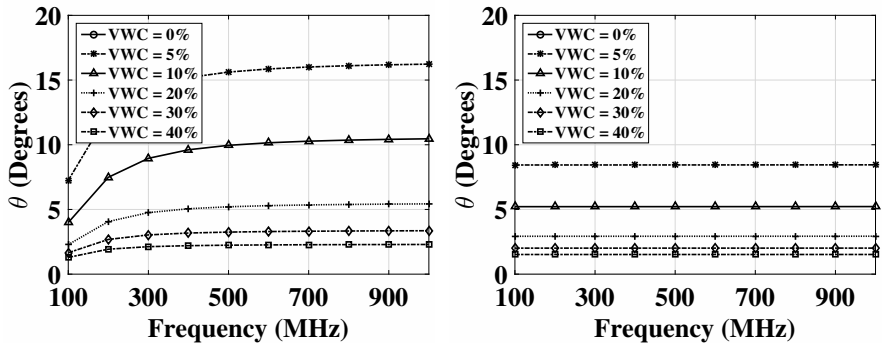

Fig. 7.8: Optimal angle at di erent frequencies in: (a) Silty Clay Loam, (b) Sandy Soil.

where the main beam peak, i.e., maximum of the array factor AF_{max}, is calculated as:

$$AF_{max} = \sum_{i=1}^{N} w_i, \tag{7.12}$$

7.3.5 SMABF Steering Algorithm

Algorithm 2 gives multiple beam patterns and meet the requirements for both communications, i.e., UG2UG and UG2AG.

7.4 Results and Optimization

This section discuss the SMABF and compares the adaptive and non-adaptive beamforming technique.

7.4.1 Optimum UG Angle

The optimum angle is determined by using equation 7.9. At optimum angle, UG communciaiton (with lateral waves) is improved adapting to soil properties. Analysis was performed on the lateral wave angle using frequency range of 100 to 1000 MHz,

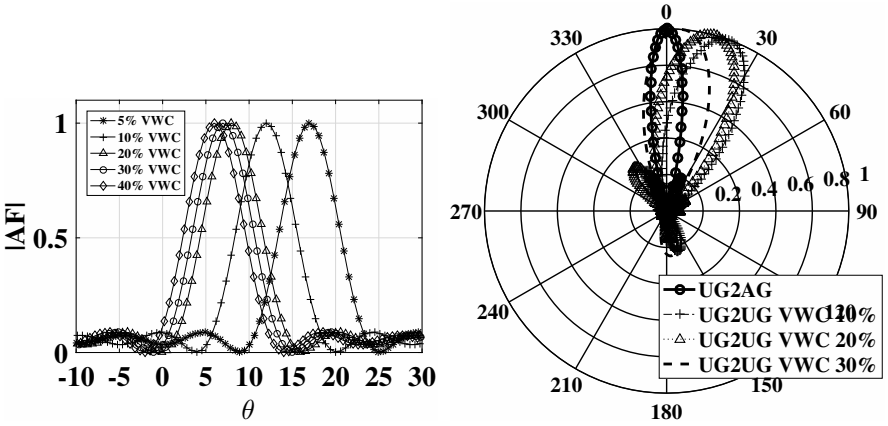

(a) (b)

Fig. 7.9: (a) Array factor for varying soil moisture levels in UG2UG communications [50], (b) Underground-to-Aboveground (UG2AG) Communications [50]

VWC between 0% to 40% and soil types of sandy and silty clay loam. Table 7.3 gives the particle distribution for both soil types.

Figs. 7.8 shows the optimal angle for varying VWC (0 to 40%) in two di erent soil types. The optimal angle in silty clay loam soil is higher than the sandy soil. The maximum optimal angle in silty clay loam soil is 16° and that in sandy soil is 9°. This is because of silty clay loam soil having higher dielectric constant than sandy soil. A decreasing trend is observed between the optimal angle and VWC, i.e., optimal angle is decreasing with increase in VWC percentage, because of increase in soil permittivity with increasing soil moisture. Table 7.2 summarizes the steering angles for both UG2UG and UG2AG communication. Fig. 7.9(a) - 7.9(b) gives the UG beam pattern with soil moisture

7.4.2 Optimum UG Angle to Enhance Lateral Wave

For validity of lateral wave communication, di erent experiments were conducted in indoor and outdoor testbed. Di erent soils are used in both testbeds: Sandy for

Table 7.3: Soil particle Size Distribution in Testbeds [145]

Textural Class	%Sand	%Silt	%Clay
Sandy Soil	86	11	3
Silty Clay Loam	13	55	32

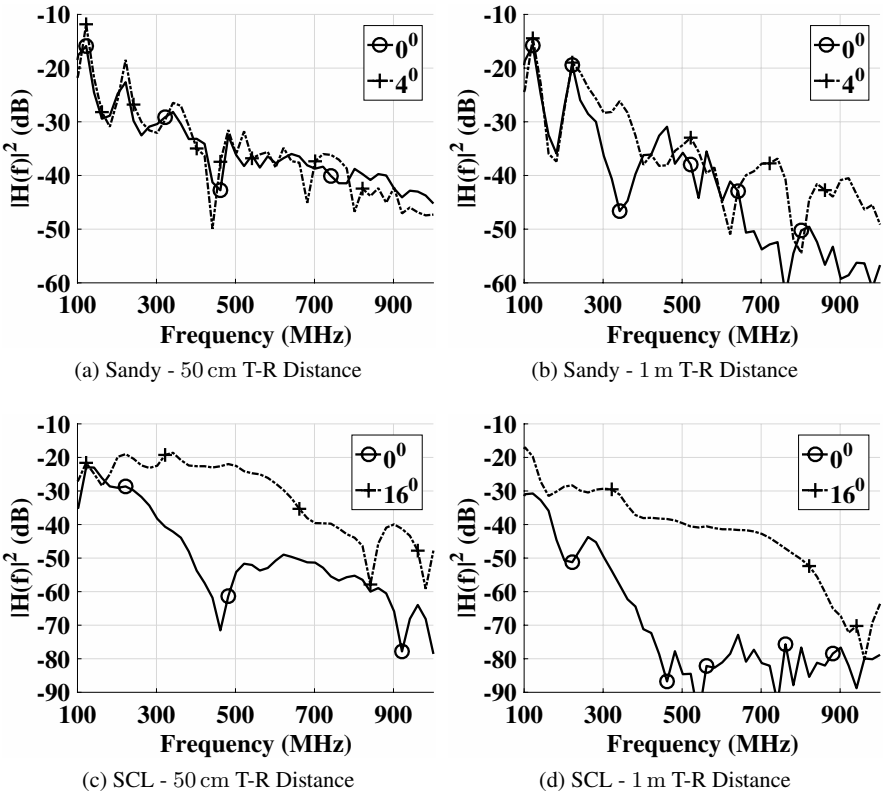

(a) Sandy - 50 cm T-R Distance

(b) Sandy - 1 m T-R Distance

(c) SCL - 50 cm T-R Distance

(d) SCL - 1 m T-R Distance

Fig. 7.10: Optimum angle in UG communication [50]: (a) Sandy Soil (50cm T-R separation), (b) Sandy Soil (1m T-R separation), (b) Silty Clay Loam Soil (50cm T-R separation), and (b) Silty Clay Loam Soil (1m T-R separation)

indoor and silty clay for outdoor. Burial depth of directional antenna is 20cm and Keysights's Fieldfox Vector Network Analyzer (VNA) N9923A is used for taking measurements. Two experiments are performed for measuring the channel gain and channel transfer function: first without changing the orientations and the other one after finding an optimum angle. For sandy soil, optimal angle is $4°$ at 37% VWC and it is $16°$ at 0% VWC for silty clay loam soil.

Figs. 7.10 shows the channel gain results for the two Transmitter-receiver (T-R) separation distances: 50cm and 1m. For a distance of 50cm, sandy soil type and a frequency of 500 MHz, a 4 dB of gain is observed at $4°$ as compared to no orientation scenario (Fig.7.10(a)). Gain is increasing with the frequency when the energy is focused at optimum angle. This is because of the reason that soil path is e ected by soil permittivity. Similarly, in Fig.7.10(b), for a distance of 1m, a higher gain is observed as compared to what was observed at 50m. This is because for large communication distances, the direct wave becomes negligible and lateral wave is significant.

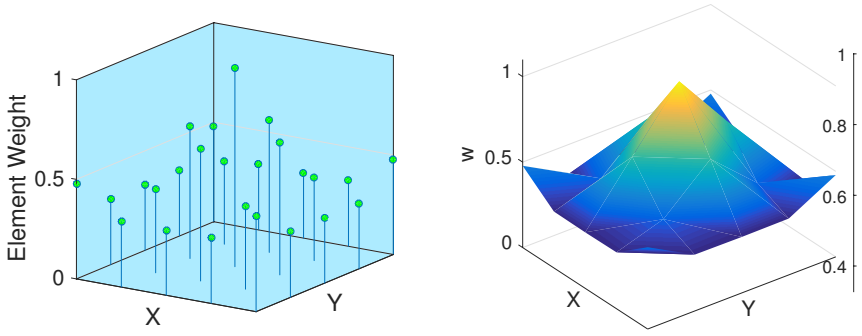

(a) (b)

Fig. 7.11: Weights of a grid element weights (433 MHz and 40% Soil moisture) [50]: (a) Stem plot (b) Surf Plot

Channel is gain is much higher in silty clay loam soil for both distances, i.e., 50cm (Fig.7.10(c)) and 1m (Fig.7.10(d)). The reason is that silty clay loam soil has high permittivity value as compared to sandy soil, hence, exhibiting higher losses and observing high channel gains.

7.4.3 Comparing SMABF with Nonadaptive Beamforming

In this section the performance of adaptive (SMABF) and non-adaptive beamforming techniques is compared. A 5×5 planar antenna array is used for the experiment and change in array factor and directivity of the antenna, due to soil moisture change, is studied in detail. Fig. 7.11 shows the elements weight of the planar antenna array at 40% VWC and frequency of 433 MHz.

Fig. 7.12 shows the array factor deterioration for silt clay loam soil and Fig. 7.13 fro sandy soil. Both results are obtain using a non-adaptive beamforming technique with VWC ranging from 5% to 40%. In both soils, the sides lobes are growing higher as the soil moisture is increasing. High soil moisture values significantly impact the wavelength of sandy soil as compared to silty clay loam soil, therefore, the e ect of high soil moisture will be severe in sandy soil as compared to silty clay loam soil.

Fig. 7.14(a) compares the directivity of adaptive SMABF with non-adaptive beamforming for both sandy and silty clay loam soils. SMABF maintains the directivity along-with the soil moisture change whereas, for non-adaptive approach, the drastic change in directivity is observed. For 5% VWC, in silty clay loam soil, non-adaptive approach has lower directivity than SMABF; For 10% and 30% VWC, in sandy soil, non-adaptive approach has same directivity as of SMABF and even shows higher directivity at 20% VWC. It is important to note that SMABF is not maximizing

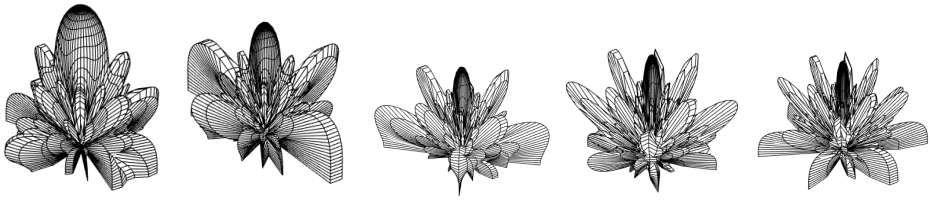

(a) 5% (b) 10% (c) 20% (d) 30% (e) 40%

Fig. 7.12: Non-adaptive Beamforming in silty clay loam soil: Array factor deterioration with changing soil moisture [50]

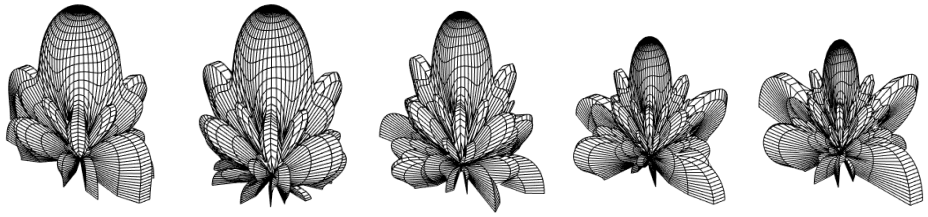

(a) 5% (b) 10% (c) 20% (d) 30% (e) 40%

Fig. 7.13: Non-adaptive Beamforming in sandy soil: Array factor deterioration with changing soil moisture [50]

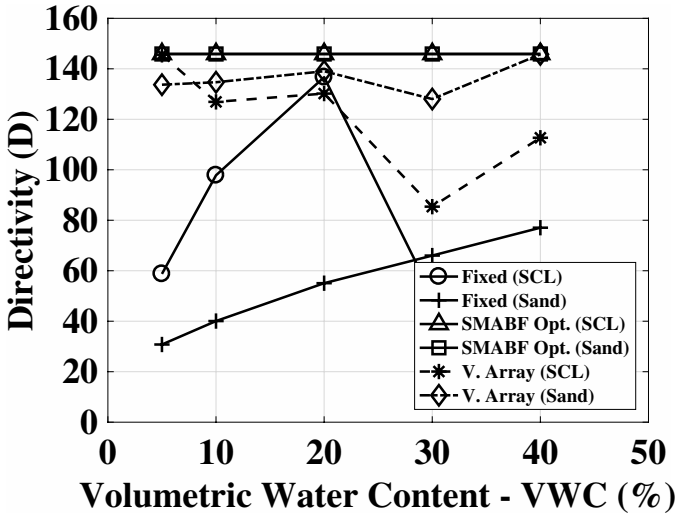

Fig. 7.14: E ect of soil moisture on directivity in sandy and SCL soil [50]

the directivity instead adapting to wavelength with change in soil moisture, however, it can be maximized by using optimal inter-element spacing.

7.4.4 Antenna Element Thinning Through Virtual Arrays

In UG array thinning, a small subset of antenna elements is selected from the full planar array using the optimization approach and a virtual array is constructed. Physical antenna elements are triggered on/o using the virtual array. This approach is used to discover the elements with optimal configuration which can be used to form current soil moisture level. Antenna element weights, w_i are toggled (on/o) as follow:

$$w_i = \begin{cases} 1 \text{ if } d = \lambda_s/2, \\ 0 \; otherwise. \end{cases} \tag{7.13}$$

where λ_s is the wavelength in soil, d is the distance between the i-th antenna element and the previous element. d is chosen in such a way that half-wavelength inter-element spacing is not disturbed due to change in soil moisture and wavelength. Table 7.4 shows change in SMABF half wavelength inter-element spacing for a frequency of 433 MHz and VWC in the range of 10% to 40%. Firstly, array uses the initial configuration for the operation and then virtual adaptive thinning is applied based on soil moisture values. Virtual SMABF maintains the side lobes and directivity and no distortion in side lobes is observed as in the case of non-adaptive beamforming.

7.4.5 SMABF Directivity Maximization

Virtual arrays have fixed directivity. This issue can be improved using directivity maximization. Goal is to optimize the inter-element spacing and avoid grating lobes. The optimization problem is given as follow:

$$\wp: \quad maxD = \frac{4\pi |AF_{max}|^2}{\int_0^{2\pi} \int_0^{\pi} |AF|^2 \sin\theta d\theta d\phi}, \tag{7.14}$$

$$s.t. \quad \frac{d}{\lambda_s} < \frac{1}{1+\sin\theta} \tag{7.15}$$

Table 7.4: SMABF half wavelength inter-element spacing (cm) for di erent VWC percentage in soil

	Volumetric Water Content (VWC)			
Soil Type	**10%**	**20%**	**30%**	**40%**
Silt Loam	30.79	23.72	20.25	18.03
Sandy	46.83	39.28	34.62	31.28
Silty Clay Loam	27.86	20.53	17.12	15.01

Table 7.5: Comparison of SMABF and UG Phased array

Property	SMABF	UG Phased Array
Inter-Element Spacing	Element Thinning Through Virtual Arrays	Depends upon soil moisture
Frequency	433 MHz	-
Directivity	Adapts to the soil moisture $\frac{4\pi\lvert AF_{max}\rvert^2}{\int_0^{2\pi}\int_0^{\pi}\lvert AF\rvert^2 \sin\theta d\theta d\phi}$	Increases with the decrease in wavelength and inter-element spacing
Steering Angle	Silt Clay Loam = 16° Sandy Soil = 9°	-
Element Weighting	Soil Moisture Adaptive weights $w^i_{sm,l+1} = w^i_{sm,l} + s(-\nabla_l)$	Soil Moisture Adaptive weights $w^i_{sm,l+1} = w^i_{sm,l} + s(-\nabla_l)$
Element Excitation	Initial distribution (w_i^0): Root matching method [12] Subsequent weights: $w_i = w_i^0 \pm \delta w_i$	Initial distribution (w_i^0): Root matching method [12] Subsequent weights: $w_i = w_i^0 \pm \delta w_i$
E ective Isotropic Radiated Power (EIRP)	-	$P_r = 10\log_{10}(10^{\frac{P_r^d}{10}} + 10^{\frac{P_r^r}{10}} + 10^{\frac{P_r^L}{10}})$
Implementation	Planar Antenna	SDR-Based Implementation

where θ is the steering angle, inter-element spacing is given by d, and D represents the directivity.

Genetic algorithms [18] is used where inter-element position can be chosen randomly or specified beforehand. A priori position can be selected without considering the soil moisture level. Inter-element spacing is then determined using a cost function.

7.4.6 Feedback Control:

Feedback signals are used to dynamically adjust the element weights through array gain feedback loops. This feedback is in addition to the weight adaption on the basis of soil moisture sensing. A pilot signal is used for maximization of array gain. SMABF transmitting array, operating in receiver mode, receives the pilot signal and based on this signal changes its parameter for the transmission. the transmitting array determine the channel state and adjust the parameters on the basis of best signal-to-noise (SNR) ratio. Fig. 7.15 shows the SMABF feedback control mechanism.

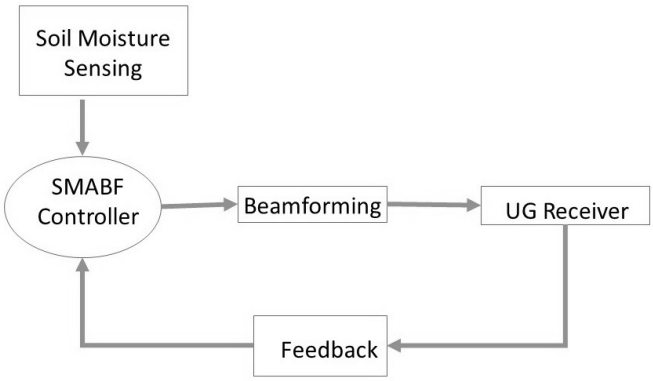

Fig. 7.15: SMABF with feedback[50]

7.4.7 Adaptive SMABF Element Weighting

Amplitude weighting [79] can be used to get a desired beam pattern from antenna elements in the array. SMABF uses the soil moisture values as an input to determine the element weight which is the reason for improved SNR in SMABF. Weight are adjusted dynamically with soil moisture for both UG2UG and UG2AG communication. These adaptive weights are given as:

$$\boldsymbol{w} = \{w_0, w_1, w_2 ... w_{n-1}\}^T \tag{7.16}$$

Change in soil moisture causes the soil permittivity to change which in turn changes the wavelength. Weight factor γ_s is given as:

$$\gamma_s = \frac{1}{\lambda_s} \times d \times \pi \times sin\theta_0 \tag{7.17}$$

Using this weight factor, adaptive weight of the i-th antenna is given as:

$$w_{sm}^i = \alpha_i exp(-j\gamma_s(2i - n - 1)) \tag{7.18}$$

where α_i represents the element coefficient. Beam patterns and required sidelobes levels are obtained using these element coefficients via positioning and element thinning technique. After determining the adaptive weight vector, desired beam pattern is obtained as:

$$F = \boldsymbol{X} w_{sm}^i \tag{7.19}$$

where $\boldsymbol{X}$ represents an intended signal. Same process is repeated using the gradient method in which adaptive weights are adjusting for upcoming iteration $(l + 1)$ as

follow [79]:

$$w^{i}_{sm,l+1} = w^{i}_{sm,l} + s(-\nabla_l) \tag{7.20}$$

where s is the stability and gradient estimate vector is given by ∇_l. Adaptive antenna array does not perform well with faster adaption rate [79]. As change in soil moisture is a slow process, this approach has minimum noise and high tolerance for performance degradation.

7.4.8 SMABF Element Excitation

Antenna element excitation also needs to be optimized as change in soil moisture can cause the performance degradation, if traditional excitation distribution methods (e.g., Hansen, Bayliss, Uniform, Dolph/Chebyshev, Binomial, Taylor, radial taper etc.). In SMABF excitation method, an initial current distribution w^0_i is determined using the root matching method [12]. New patterns are determines for each soil moisture change. Due to slow pace soil moisture change, patterns di ers from each other in small angle steps. The changes in w_i are given by δw_i:

$$w_i = w^0_i \pm \delta w_i \tag{7.21}$$

With the knowledge of desired and current patterns, matrix inversion method is used to solve pattern di erence equation for getting δw_i. This δw_i is used for calculating new distribution for new beam pattern. The process is repeated multiple times until the desired beam pattern is obtained.

7.4.9 Simulations

A simulation program, CST Microwave Studio (MWS), is used to simulate SMABF design. A 5×5 phased array in sandy soil is used for the simulation. The operating frequency of the array lies between 0.2 - 0.6 GHz with beam steering support for di erent communication types and angles given in Table 7.2. Operating bandwidth, S-parameters and radiation pattern of an array depends upon the individual element, therefore, to analyze these parameters, a single dipole antenna is simulated initially. The simulation with dipole antenna is performed using resonant frequency of 433 MHz and Feed impedance of $50\,\Omega$. Elements are simulated as PEC cylindrical material and these elements are excited using the gap between the spacing of elements. Simulated S-parameter values are compared with measure S-parameter values for validation. Both results are discussed in Section 7.2.3 and confirms each other. Simulated results shows that change in soil moisture e ects the resonant frequency, bandwidth, and reflection coefficient. More details on this e ect are given in Section 7.2.3).

After verifying the design of individual element, full array is simulated for the validation. Fig. 7.16(a) shows the structure of simulated array. Distribution matrix

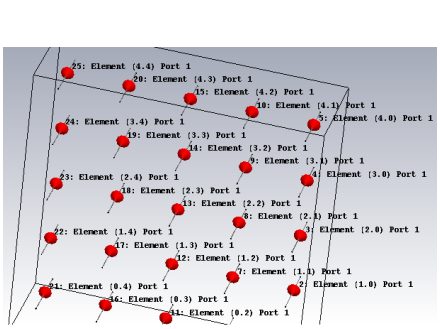

(a)

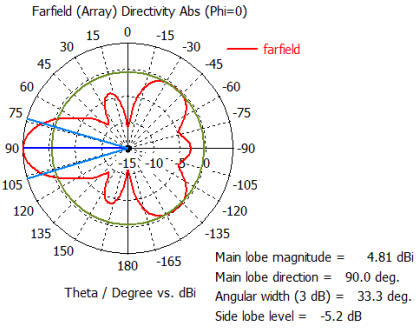

(b)

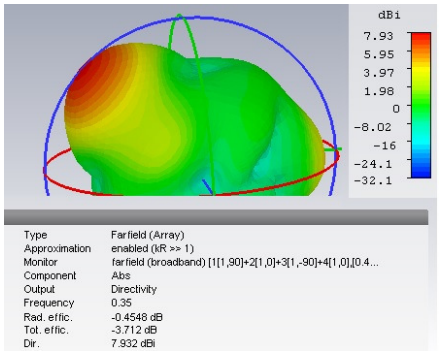

(c)

Fig. 7.16: (a) Design of 5×5 array in CST MWS [50], (b) UG2AG far-field simulated in CST MWS [50], (c) 3D view of UG2AG Beam [50]

are estimated after giving the beam pattern specification for UG2UG and UG2AG communication. The matrix is used for exciting the element and obtaining the desired beam pattern. The distribution matrix is recalculated for every variation in soil moisture. Accordingly, beam steering angle is adjusted and the process is repeated multiple times to adapt to soil moisture changes. Fig. 7.16(b) shows the UG2AG results for the simulation with beam parameters and Fig. 7.16(c) shows in same in 3D. It is observed that simulation results confirms the beam synthesis analysis from Section. 7.3.

7.5 Underground Phased Array Antennas

Underground transmitter, with phased array antennas, uses UG transmit beamforming to maximize contribution of lateral wave by using a particular angle to transmit energy [50], [47, 145]. This saves energy loss by using narrow-width beam instead of transmitting signal in isotropic direction. The primary goals of wireless underground communications are: a) increase the received signal strength, and b) minimize the interference at receiver end [50, 51].

Soil uses weights which adapts to the soil moisture values of the soil. Moreover, UG phased antenna arrays uses array gain feedback loops as feedback signals to adjust weights. This is done to maximize the array gain with pilot signals. This method uses the phased array antenna transmitter for receiving the pilot signal (as a receiver) and adjusts parameter for transmission of the signal as a transmitter. While transmitter is working in a receiver mode, channel state is estimated by changing the scan angles. The best SNIR values are selected and soil moisture values are changed to adjust the parameters. Fig. 7.15 shows soil moisture-adaptive feedback controller with the feedback.

7.5.1 Adaptive Element Weighting

The array elements signals of beamforming antennas can be controlled to produce the desired beam by phase and amplitude weighting [71, 79]. In UG phased arrays, the current environment and the soil moisture information is used to weight the elements which leads to improvements in received SNR. The adaptive weight adjustment is done to keep the desired UG2UG and UG2AG characteristics based on the soil moisture variations.

Soil moisture adaptive weights are expressed as:

$$\boldsymbol{w} = \{w_0, w_1, w_2 ... w_{n-1}\}^T \tag{7.22}$$

The permittivity of the soil changes with the change in soil moisture and hence the wavelength. The weight factor γ_s is defined as:

$$\gamma_s = \frac{1}{\lambda_s} \times d \times \pi \times sin\theta_0 \tag{7.23}$$

where d is the inter-element distance. Accordingly, with this weight factor, i^{th} soil moisture adaptive weight w_{sm}^i becomes:

$$w_{sm}^i = \alpha_i exp(-j\gamma_s(2i - n - 1)) \tag{7.24}$$

where α_i is the element coefficient. These element coefficients are optimized to obtain desired sidelobe levels and beam patterns through element thinning and positioning approach. Once the beamforming vector is populated with the adaptive weights, the

desired beam pattern is produced as following:

$$F = \boldsymbol{X} w_{sm}^{i} \tag{7.25}$$

where $\boldsymbol{X}$ is the intended signal. To repeat this process with soil moisture change, gradient method is used. In this method, soil moisture adaptive weights are adjusted for next $(l+1)$ iteration as as [50, 79]:

$$w_{sm,l+1}^{i} = w_{sm,l}^{i} + s(-\nabla_l) \tag{7.26}$$

where s ensures stability and convergence and ∇_l is the gradient estimate vector. It is well known that performance of an adaptive antenna array system degrades with faster adaption [27, 79]. Since the soil moisture is a slowly varying process, this simple-to-implement approach exhibits minimum noise and high tolerance to performance degradation that is caused by faster adoption and limited sampling.

7.5.2 Phased Array Element Excitation

In addition to wavelength, and element position optimization, current excitation also need to be optimized. Due to the soil moisture variations, the use of conventional excitation distributions (e.g., Uniform, Dolph/Chebyshev, Binomial, Taylor, Hansen, Tseng, Bayliss, separable, radial taper, and radial taper squared) lead to degraded beam patterns with soil moisture variations [34, 44, 79]. Therefore, in this section we develop a soil moisture adaptive phased array excitation method to maintain the desired pattern. This method works as follows [20, 41].

First, an initial current distribution w_i^0 is found for the desired pattern by using the root matching method [12, 25, 30]. Once the soil moisture changes, the new patten is determined. The soil moisture does not vary drastically with time in the field. Therefore, with change in soil moisture, the new pattern vary gradually from the old one in small angle steps. Hence, the w_i is expressed in minor variations δw_i to the w_i^0:

$$w_i = w_i^0 \pm \delta w_i \tag{7.27}$$

Since the current and desirable patterns are known, the pattern di erence equation is solved using the matrix inversion method to obtain the δw_i. Accordingly, it is used to get the new current which defines new pattern. This method is repeated iteratively until the desired beam pattern is achieved. To further improve the pattern, a received power based feedback method can be employed which will enhance performance and converge faster. The received power and the directivity are defined in the next section.

7.5.3 Effective Isotropic Radiated Power (EIRP)

The phased array e ective isotropic radiated power (EIRP) is expressed as the product of the transmitted power and antenna gain:

$$P_{rad} = G_t P_t, \tag{7.28}$$

where P_t is the transmitted power and G_t is the array gain.

The far-field power density P_{av} is expressed as [61]:

$$P_{av} = P_{av}^{D} + P_{av}^{R} + P_{av}^{L} \, . \tag{7.29}$$

where D (direct), R (reflected), L (lateral) denotes the power densities of corresponding wave component [48, 59]. The received power is the product of far-field power density P_{av} and antenna aperture ($\lambda_s^2/4\pi$). The received power is calculated as [55, 61]:

$$\begin{aligned} P_r^d &= P_t + 20\log_{10}\lambda_s - 20\log_{10} r_1 - 8.69\alpha_s r_1 \\ &\quad -22 + 10\log_{10} D_{rl} \, , \\ P_r^r &= P_t + 20\log_{10}\lambda_s - 20\log_{10} r_2 - 8.69\alpha_s r_2 \\ &\quad +20\log_{10}\Gamma - 22 + 10\log_{10} D_{rl} \, , \\ P_r^L &= P_t + 20\log_{10}\lambda_s - 40\log_{10} d - 8.69\alpha_s(h_t + h_r) \\ &\quad +20\log_{10} T - 22 + 10\log_{10} D_{rl} \, , \end{aligned} \tag{7.30}$$

where Γ and T are reflection and transmission coefficients [28, 61], and λ_s is the wavelength in soil. The received power, for an isotropic antenna, is expressed as [46, 54, 61]:

$$P_r = 10\log_{10}(10^{\frac{P_r^d}{10}} + 10^{\frac{P_r^r}{10}} + 10^{\frac{P_r^L}{10}}) \, . \tag{7.31}$$

The directivity of the underground phased array antenna is defined as [50, 72]:

$$D = \frac{4\pi |AF_{max}|^2}{\int_0^{2\pi}\int_0^{\pi} |AF|^2 \sin\theta d\theta d\phi}, \tag{7.32}$$

where the AF_{max} is the maximum of the array factor [26, 35, 50].

7.6 Beyond Optimal: Enhancement of Array Dimensions

This section discuss performance of UG phased array through directivity settings [50, 52]. Figs. 7.17 plots the change in directivity with deployment at 30% moisture level. It also observe the e ect of extending array dimension by increasing number of elements. It concludes that inter-element spacing must increase with low soil

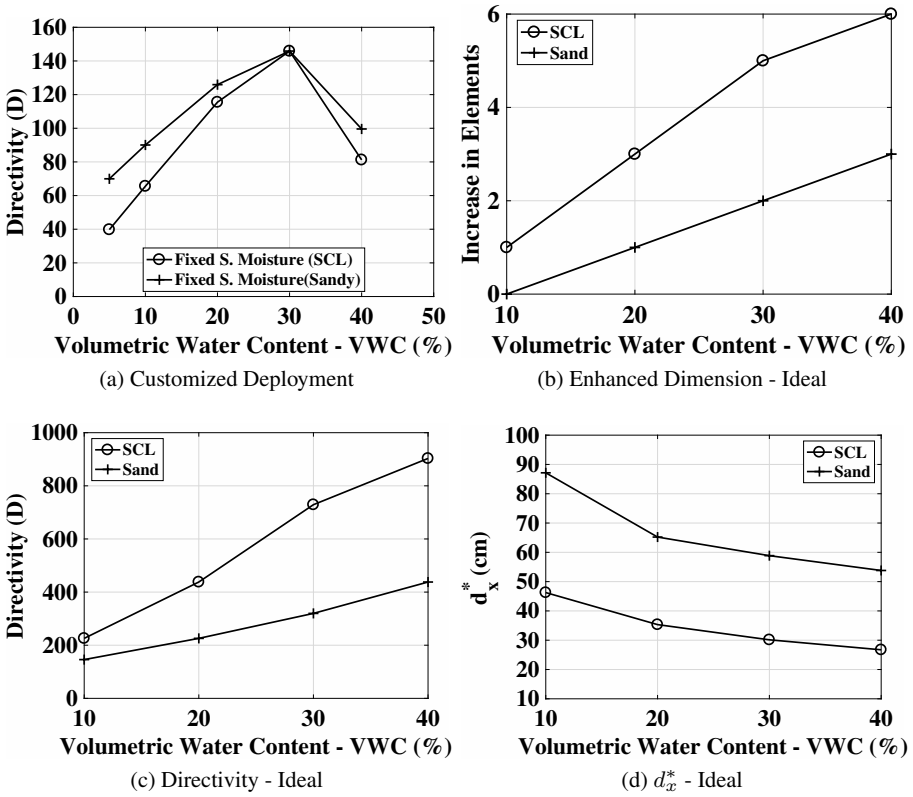

(a) Customized Deployment (b) Enhanced Dimension - Ideal

(c) Directivity - Ideal (d) d_x^* - Ideal

Fig. 7.17: (a) Directivity at 30% soil moisture level for optimized deployment, Enhanced array dimension: (b) Number of elements, (c) Directivity, (d) d_x^*.

moisture levels. Increasing the inter-element spacing also increases the overall array dimension. Moreover, if the soil moisture is decreased for virtual array scenarios with fixed (e.g., 5×5) configuration, then array size also decreases despite maintaining optimum value of directivity. However, at the same time, fixed configuration (5×5) at high soil moisture levels results in wastage of resources, i.e., elements over fixed dimensions. For high soil moisture levels, UG phased array performance is improved by using more elements, hence, getting beyond optimum directivity [32, 45].

An ideal case is considered first where an array (5×5) is designed with optimum inter-element spacing d_x^* at 5% soil moisture levels. This configuration is used for both types of soils. This design gives the maximum possible physical dimensions. After that, if the soil moisture level is increased, number of elements are determined and deployed within these fixed physical dimensions. It is also important to note that no limitation is placed on practical inter-element spacing d_x. The increased number of elements, within fixed maximum dimension, are also computed using d_x^* of the

current soil moisture level. For second case, practical limitations are applied on d_x, and performance of the system is studied [24, 31].

Fig. 7.17(b) plots the e ect of increased element in 5×5 array along with increasing soil moisture level. The experiment is performed in both types of soil. In silt clay loam soil, at all soil moisture levels array dimension is enhanced to 6×6, 8×8, 10×10, and 11×11 for addition of 1, 3, 5, and 6 elements at soil moisture level of 10%, 20%, 30%, and 40%, respectively. In sandy soil, the array dimension is not e ected at soil moisture level of 10% , however, it is enhanced to 6×6, 7×7, and 8×8 at soil moisture level of 20%, 30%, and 40%, respectively.

Fig. 7.17(c) plots the directivity of enhanced configuration. For silt clay loam soil, at higher soil moisture level, the directivity is increased significantly with enhanced configuration. This happens because of two reasons: a) decrease in wavelength when soil moisture levels are increase, and b) smaller inter-element spacing d_x^* in silt clay loam soil (see Fig. 7.17(d)) results in increased number of elements in array dimensions which in-turn increase its directivity in silt clay loam soil. Hence, enhanced array deployment can be advantageous for the soil with higher clay content and high soil moisture level [29, 65].

7.7 Antenna Array Implementation

This section discusses UG phased array in the context of software and hardware implementation.

7.7.1 Software Defined Implementation

Evolution in SDR-based technology has enable the robust UG phased arrays implementations. Software-defined array elements allows development of steering solutions with the ability to process complex algorithms. These steering solutions can be used by antenna elements to communicate with static and mobile AG nodes. SDR-based UG beamforming [28] faces various challenges for its implementation. Among all challenges, di erent phase shifts of antenna element is the major one. A desired beam pattern requires same phase shift for all antenna element in a particular direction. This can be done by doing proper calibration of phase shifter, real-time synchronization and phase correction for the all elements.

Soil moisture-based digital beamforming method uses planar antenna array. It consists of its own phase-shifter and is programmed on pre-defined communication parameters for communicating with the UG and AG arrays. Multiple beams can be stitched in such a way that the total number of beam patterns can be calculated after analyzing the UG and AG devices and can be stored in a database for later use [43].

SDR-based phase shifting approach dynamically adapts to the wavelength with the change in soil moisture values. The processing is done in the software defined

radios. Major benefit of this technique is that it adapts to for the uncertainties of UG environment without changing the arrangement of the antenna array, hence, consuming less energy as compared to traditional mechanical techniques [13, 33].

7.7.2 Hardware Components

Hardware-based solutions for UG phased array includes using dipole antenna elements and printed circuit antenna elements. Moreover, other microwave components, e.g., amplifiers, phase shifters, dividers and hybrids can be used as printed circuits [13, 36, 53]. To achieve a good wideband properties, a stripline configuration includes using a closely spaced antenna elements with large diameter. A prototype system can be designed and tested using EM-based simulations. The performance of an antenna array su ers at the edges. This can be avoided using resistive elements as a dummy element at the edge. Using the results from the simulation-based design, an initial array layout can b configured. This layout can be optimized using vector network analyzer [37, 40].

7.8 Future Directions

As a future research direction, e ect of soil-air interface on communication performance of UG phased array should be investigated in detail. Reflection from the interface can be studies by adjusting the array factor. Moreover, receiving array should also be analyzed in context of mutual coupling between array elements, antenna reciprocity principal, impedance matching, and simultaneous sending and receiving functionality [38, 39, 42].

It is important to realize UG phased array with soil moisture sensing capabilities. It is a challenging task incurring more complexity in the system. UG phased antenna array is an enabling technology for th next-generation wireless UG systems due to its decrease cost, lower hardware complexity, extended communication range and high data rate. It can be considered as a serious contender to replace traditional OTA solutions.

References

[52] Akyildiz IF, Stuntebeck EP (2006) Wireless underground sensor networks: Research challenges. Ad Hoc Networks Journal

[54] Akyildiz IF, Sun Z, Vuran MC (2009) Signal propagation techniques for wireless underground communication networks. Physical Communication Journal (Elsevier) 2(3):167–183

[3] Alexandropoulos GC, Ferrand P, m Gorce J, Papadias CB (2016) Advanced coordinated beamforming for the downlink of future lte cellular networks. IEEE Communications Magazine DOI 10.1109/MCOM.2016.7509379
[4] Anand N, Lee SJ, Knightly EW (2012) Strobe: Actively securing wireless communications using zero-forcing beamforming. In: INFOCOM, 2012 Proceedings IEEE, pp 720–728, DOI 10.1109/INFCOM.2012.6195817
[5] Aryafar E, etal (2013) Adam: An adaptive beamforming system for multicasting in wireless lans. IEEE/ACM Trans on Networking DOI 10.1109/TNET.2012.2228501
[58] Bogena HR, Herbst M, Huisman JA, Rosenbaum U, Weuthen A, Vereecken H (2010) Potential of wireless sensor networks for measuring soil water content variability. Vadose Zone Journal
[7] Dobson M, etal (1985) Microwave dielectric behavior of wet soil—Part II: Dielectric mixing models. IEEE Trans Geoscience and Remote Sensing GE-23(1):35 –46, DOI 10.1109/TGRS.1985.289498
[61] Dong X, Vuran MC (2011) A channel model for wireless underground sensor networks using lateral waves. In: Proc. of IEEE Globecom '11, Houston, TX
[62] Dong X, Vuran MC (2013) Impacts of soil moisture on cognitive radio underground networks. In: Proc. IEEE BlackSeaCom, Georgia
[9] Dong X, Vuran MC, Irmak S (2012) Autonomous precision agricultrue through integration of wireless underground sensor networks with center pivot irrigation systems. Ad Hoc Networks (Elsevier)
[11] Du Y, etal (2014) iBeam: Intelligent client-side multi-user beamforming in wireless networks. In: IEEE INFOCOM 2014, DOI 10.1109/INFOCOM.2014.6848009
[12] Elliott RS (1981) Antenna Theory and Design. Prentice-Hall, Inc.
[13] Fenn A, Hurst P (2015) Ultrawideband Phased Array Antenna Technology for Sensing and Communications Systems. MIT Press
[14] Godara LC (1997) Application of antenna arrays to mobile communications. ii. beam-forming and direction-of-arrival considerations. Proceedings of the IEEE 85(8):1195–1245, DOI 10.1109/5.622504
[15] Gross F (2015) Smart Antennas with MATLAB. McGraw-Hill
[75] Guo H, Sun Z (2014) Channel and energy modeling for self-contained wireless sensor networks in oil reservoirs. IEEE Trans Wireless Communications 13(4):2258–2269, DOI 10.1109/TWC.2013.031314.130835
[17] Hansen R (2009) Phased Array Antennas. Wiley
[18] Haupt R (2015) Timed Arrays. Wiley
[19] King RWP, Smith G (1981) Antennas in Matter. MIT Press
[20] King RWP, Owens M, Wu TT (1992) Lateral Electromagnetic Waves. Springer-Verlag
[21] Kissele S, Akyildiz IF, Gerstacker W (2015) Beamforming for magnetic induction based wireless power transfer systems with multiple receivers. In: 2015 IEEE GLOBECOM, DOI 10.1109/GLOCOM.2015.7417006
[20] Konda A, Rau A, Stoller MA, Taylor JM, Salam A, Pribil GA, Argyropoulos C, Morin SA (2018) Soft microreactors for the deposition of conductive metallic

traces on planar, embossed, and curved surfaces. Advanced Functional Materials 28(40):1803020, DOI 10.1002/adfm.201803020
[23] Kontaxis D, etal (2016) Optimality of transmit beamforming in spatially correlated mimo rician fading channels. Wir Per Comm
[24] Lakshmanan S, Sundaresan K, Kokku R, Khojestepour A, Rangarajan S (2009) Towards adaptive beamforming in indoor wireless networks: An experimental approach. In: INFOCOM 2009, IEEE, DOI 10.1109/INFCOM.2009.5062199
[25] Mailloux R (2005) Phased Array Antenna Handbook. Artech House
[100] Markham A, Trigoni N (2012) Magneto-inductive networked rescue system (miners): Taking sensor networks underground. In: Proceedings of the 11th ICPS, ACM, IPSN '12, pp 317–328, DOI 10.1145/2185677.2185746
[27] Nitsche T, etal (2015) Steering with eyes closed: Mm-wave beam steering without in-band measurement. In: IEEE INFOCOM, DOI 10.1109/INFOCOM.2015.7218630
[28] Quitin F, etal (2013) A scalable architecture for distributed transmit beamforming with commodity radios: Design and proof of concept. IEEE Trans on Wireless Communications DOI 10.1109/TWC.2013.012513.121029
[24] Salam A (2018) Pulses in the sand: Long range and high data rate communication techniques for next generation wireless underground networks. ETD collection for University of Nebraska - Lincoln (AAI10826112), URL http://digitalcommons.unl.edu/dissertations/AAI10826112
[25] Salam A (2019) A comparison of path loss variations in soil using planar and dipole antennas. In: 2019 IEEE International Symposium on Antennas and Propagation, IEEE
[26] Salam A (2019) Design of subsurface phased array antennas for digital agriculture applications. In: Proc. 2019 IEEE International Symposium on Phased Array Systems and Technology (IEEE Array 2019), Waltham, MA, USA
[27] Salam A (2019) A path loss model for through the soil wireless communications in digital agriculture. In: 2019 IEEE International Symposium on Antennas and Propagation, IEEE, pp 1–2
[28] Salam A (2019) Sensor-free underground soil sensing. In: ASA, CSSA and SSSA International Annual Meetings (2019), ASA-CSSA-SSSA
[29] Salam A (2019) Subsurface mimo: A beamforming design in internet of underground things for digital agriculture applications. Journal of Sensor and Actuator Networks 8(3), DOI 10.3390/jsan8030041, URL https://www.mdpi.com/2224-2708/8/3/41
[30] Salam A (2019) Underground Environment Aware MIMO Design Using Transmit and Receive Beamforming in Internet of Underground Things, Springer International Publishing, Cham, pp 1–15
[31] Salam A (2019) An underground radio wave propagation prediction model for digital agriculture. Information 10(4):147
[32] Salam A (2019) Underground soil sensing using subsurface radio wave propagation. In: 5th Global Workshop on Proximal Soil Sensing, Columbia, MO

[33] Salam A (2020) Internet of Things for Environmental Sustainability and Climate Change, Springer International Publishing, Cham, pp 33–69. DOI 10.1007/978-3-030-35291-2_2, URL https://doi.org/10.1007/978-3-030-35291-2_2

[34] Salam A (2020) Internet of Things for Sustainability: Perspectives in Privacy, Cybersecurity, and Future Trends, Springer International Publishing, Cham, pp 299–327. DOI 10.1007/978-3-030-35291-2_10, URL https://doi.org/10.1007/978-3-030-35291-2_10

[35] Salam A (2020) Internet of Things for Sustainable Community Development, 1st edn. Springer Nature, DOI 10.1007/978-3-030-35291-2

[36] Salam A (2020) Internet of Things for Sustainable Community Development: Introduction and Overview, Springer International Publishing, Cham, pp 1–31. DOI 10.1007/978-3-030-35291-2_1, URL https://doi.org/10.1007/978-3-030-35291-2_1

[37] Salam A (2020) Internet of Things for Sustainable Forestry, Springer International Publishing, Cham, pp 147–181. DOI 10.1007/978-3-030-35291-2_5, URL https://doi.org/10.1007/978-3-030-35291-2_5

[38] Salam A (2020) Internet of Things for Sustainable Human Health, Springer International Publishing, Cham, pp 217–242. DOI 10.1007/978-3-030-35291-2_7, URL https://doi.org/10.1007/978-3-030-35291-2_7

[39] Salam A (2020) Internet of Things for Sustainable Mining, Springer International Publishing, Cham, pp 243–271. DOI 10.1007/978-3-030-35291-2_8, URL https://doi.org/10.1007/978-3-030-35291-2_8

[40] Salam A (2020) Internet of Things for Water Sustainability, Springer International Publishing, Cham, pp 113–145. DOI 10.1007/978-3-030-35291-2_4, URL https://doi.org/10.1007/978-3-030-35291-2_4

[41] Salam A (2020) Internet of Things in Agricultural Innovation and Security, Springer International Publishing, Cham, pp 71–112. DOI 10.1007/978-3-030-35291-2_3, URL https://doi.org/10.1007/978-3-030-35291-2_3

[42] Salam A (2020) Internet of Things in Sustainable Energy Systems, Springer International Publishing, Cham, pp 183–216. DOI 10.1007/978-3-030-35291-2_6, URL https://doi.org/10.1007/978-3-030-35291-2_6

[43] Salam A (2020) Internet of Things in Water Management and Treatment, Springer International Publishing, Cham, pp 273–298. DOI 10.1007/978-3-030-35291-2_9, URL https://doi.org/10.1007/978-3-030-35291-2_9

[44] Salam A (2020) Wireless underground communications in sewer and stormwater overflow monitoring: Radio waves through soil and asphalt medium. Information 11(2)

[45] Salam A, Karabiyik U (2019) A cooperative overlay approach at the physical layer of cognitive radio for digital agriculture

[46] Salam A, Shah S (2019) Internet of things in smart agriculture: Enabling technologies. In: 2019 IEEE 5th World Forum on Internet of Things (WF-IoT), IEEE, pp 692–695

[139] Salam A, Vuran MC (2016) Impacts of soil type and moisture on the capacity of multi-carrier modulation in internet of underground things. In: Proc. ICCCN 2016, Waikoloa, Hawaii, USA

[47] Salam A, Vuran MC (2016) Impacts of soil type and moisture on the capacity of multi-carrier modulation in internet of underground things. In: Proc. of the 25th ICCCN 2016, Waikoloa, Hawaii, USA

[48] Salam A, Vuran MC (2017) Em-based wireless underground sensor networks pp 247–285, DOI 10.1016/B978-0-12-803139-1.00005-9

[50] Salam A, Vuran MC (2017) Smart underground antenna arrays: A soil moisture adaptive beamforming approach. In: Proc. 36th IEEE INFOCOM 2017, Atlanta, USA

[56] Salam A, Vuran MC (2017) Wireless underground channel diversity reception with multiple antennas for internet of underground things. In: Proc. IEEE ICC 2017, Paris, France

[50] Salam A, Vuran MC (2017) Wireless underground channel diversity reception with multiple antennas for internet of underground things. In: Proc. IEEE ICC 2017, Paris, France

[58] Salam A, Vuran MC (2018) EM-Based Wireless Underground Sensor Networks. In: Pamukcu S, Cheng L (eds) Underground Sensing, Academic Press, pp 247 – 285, DOI https://doi.org/10.1016/B978-0-12-803139-1.00005-9

[59] Salam A, Vuran MC, Irmak S (2016) Pulses in the sand: Impulse response analysis of wireless underground channel. In: Proc. IEEE INFOCOM 2016, San Francisco, USA

[51] Salam A, Vuran MC, Irmak S (2016) Pulses in the sand: Impulse response analysis of wireless underground channel. In: The 35th Annual IEEE International Conference on Computer Communications (INFOCOM 2016), San Francisco, USA

[145] Salam A, Vuran MC, Irmak S (2016) Pulses in the sand: Impulse response analysis of wireless underground channel. In: Proc. IEEE INFOCOM 2016, San Francisco, USA

[62] Salam A, Vuran MC, Irmak S (2017) Towards internet of underground things in smart lighting: A statistical model of wireless underground channel. In: Proc. 14th IEEE International Conference on Networking, Sensing and Control (IEEE ICNSC), Calabria, Italy

[52] Salam A, Vuran MC, Irmak S (2017) Towards internet of underground things in smart lighting: A statistical model of wireless underground channel. In: Proc. 14th IEEE International Conference on Networking, Sensing and Control (IEEE ICNSC), Calabria, Italy

[53] Salam A, Hoang AD, Meghna A, Martin DR, Guzman G, Yoon YH, Carlson J, Kramer J, Yansi K, Kelly M, et al. (2019) The future of emerging iot paradigms: Architectures and technologies

[54] Salam A, Vuran MC, Dong X, Argyropoulos C, Irmak S (2019) A theoretical model of underground dipole antennas for communications in internet of underground things. IEEE Transactions on Antennas and Propagation

[55] Salam A, Vuran MC, Irmak S (2019) Di-sense: In situ real-time permittivity estimation and soil moisture sensing using wireless underground communications. Computer Networks 151:31 – 41, DOI https://doi.org/10.1016/j.comnet.2019.01.001, URL http://www.sciencedirect.com/science/article/pii/S1389128618303141

[67] Staiman D, Tamir T (1966) Nature and optimisation of the ground (lateral) wave excited by submerged antennas. Electrical Engineers, Proceedings of the Institution of 113(8), DOI 10.1049/piee.1966.0220

[164] Sun Z, Akyildiz I (2010) Channel modeling and analysis for wireless networks in underground mines and road tunnels. IEEE Trans on Communications DOI 10.1109/TCOMM.2010.06.080353

[69] Sun Z, Akyildiz I (2010) Magnetic induction communications for wireless underground sensor networks. Antennas and Propagation, IEEE Transactions on 58(7):2426–2435, DOI 10.1109/TAP.2010.2048858

[70] Sun Z, etal (2011) MISE-PIPE: MI based wireless sensor networks for underground pipeline monitoring. Ad Hoc Networks

[71] Sun Z, Wang P, Vuran MC, Al-Rodhaan MA, Al-Dhelaan AM, Akyildiz IF (2011) Border patrol through advanced wireless sensor networks. Ad Hoc Networks 9(3):468–477

[170] Tan X, Sun Z, Akyildiz IF (2015) Wireless underground sensor networks: MI-based communication systems for underground applications. IEEE Antennas and Propagation Magazine 57(4), DOI 10.1109/MAP.2015.2453917

[65] Temel S, Vuran MC, Lunar MM, Zhao Z, Salam A, Faller RK, Stolle C (2018) Vehicle-to-barrier communication during real-world vehicle crash tests. Computer Communications 127:172–186

[74] Tiusanen MJ (2006) Wideband antenna for underground Soil Scout transmission. IEEE Antennas and Wireless Propagation Letters 5(1):517–519

[177] Vuran MC, Akyildiz IF (2010) Channel model and analysis for wireless underground sensor networks in soil medium. Physical Communication 3(4):245–254, DOI DOI:10.1016/j.phycom.2010.07.001

[71] Vuran MC, Dong X, Anthony D (2015) Antenna for wireless underground communication. URL http://www.google.com/patents/US20150181315, uS Patent App. 14/415,455

[71] Vuran MC, Salam A, Wong R, Irmak S (2018) Internet of underground things in precision agriculture: Architecture and technology aspects. Ad Hoc Networks DOI https://doi.org/10.1016/j.adhoc.2018.07.017, URL http://www.sciencedirect.com/science/article/pii/S1570870518305067

[72] Vuran MC, Salam A, Wong R, Irmak S (2018) Internet of underground things: Sensing and communications on the field for precision agriculture. In: 2018

IEEE 4th World Forum on Internet of Things (WF-IoT) (WF-IoT 2018), , Singapore

[79] Widrow B, etal (1967) Adaptive antenna systems. Proceedings of the IEEE DOI 10.1109/PROC.1967.6092